RMetS
Royal Meteorological Society

The Gulf Stream influence on wintertime North Atlantic jet variability

Christopher H. O'Reilly,[a]* Shoshiro Minobe,[b] Akira Kuwano-Yoshida[c] and Tim Woollings[a]
[a]*Department of Physics, Atmospheric, Oceanic and Planetary Physics, University of Oxford, UK*
[b]*Department of Natural History Sciences, Graduate School of Science, Hokkaido University, Japan*
[c]*Application Laboratory, Japan Agency for Marine-Earth Science and Technology, Yokosuka, Japan*

*Correspondence to: C. H. O'Reilly, Department of Physics, Atmospheric, Oceanic and Planetary Physics, University of Oxford, Oxford OX1 3PU, UK. E-mail: christopher.oreilly@physics.ox.ac.uk

In this article we investigate the influence of the Gulf Stream sea-surface temperature (SST) front on the North Atlantic eddy-driven jet and its variability, by analysing the NCEP-CFSR dataset and a pair of AGCM simulations forced with realistic and smoothed Gulf Stream SST boundary conditions. The Gulf Stream SST front acts to generate stronger meridional eddy heat flux in the lower troposphere and an eddy-driven jet over the eastern North Atlantic which is located further polewards than in the simulation with smoothed SST. The strong Gulf Stream SST gradient is found to be crucial in more accurately capturing the trimodal distribution of the eddy-driven jet latitude, with the more poleward climatological jet being the result of the jet occupying the northern jet position more frequently in the simulation forced with observed SSTs. The more frequent occurrence of the northern jet location is associated with periods of high eddy heat flux over the Gulf Stream region. Composite analysis of high eddy heat flux events reveals that the significantly higher heat flux is followed by larger and more persistient poleward jet excursions in the simulations with realistic SSTs than in the simulation with smoothed SSTs, with upper-tropospheric eddy momentum fluxes acting to maintain the more poleward eddy-driven jet. Periods of high eddy heat flux over the Gulf Stream region are also shown to be associated with increased blocking frequency over Europe, which are clearly distinct from periods with a northern jet position.

Key Words: storm track; North Atlantic jetstream; eddy-driven jet; Gulf Stream; blocking

Received 11 April 2016; Revised 30 July 2016; Accepted 22 August 2016; Published online in Wiley Online Library 11 October 2016

1. Introduction

Jet streams play an important role in determining the weather and climate of the midlatitudes. Jet streams are generally characterised according to the mechanisms by which they arise. Subtropical jets occur on the poleward flanks of the Hadley cells, in the upper troposphere, where a westerly jet occurs due to the angular momentum conservation of the poleward moving air (e.g. Held and Hou, 1980). Eddy-driven jets occur along the midlatitude storm tracks, where synoptic-scale eddies generate momentum flux convergence (e.g. Hoskins *et al.*, 1983). Whereas subtropical jets are confined to the upper troposphere, eddy-driven jets extend through the entire depth of the troposphere and are responsible for the prevailing surface westerlies. Whilst subtropical and eddy-driven jets are usually not clearly separated, they tend to be well separated over the North Atlantic in winter, where thermal forcing of the subtropical jet is relatively weak (Li and Wettstein, 2012) and intense storm track activity generates a strong eddy-driven jet in the extratropics.

Wintertime variability of the eddy-driven jet over the North Atlantic and Europe is strongly related to the North Atlantic Oscillation (NAO). However, since the nature of the NAO largely represents the position and persistence of the eddy-driven jet (e.g. Lorenz and Hartmann, 2003; Eichelberger and Hartmann, 2007; Vallis and Gerber, 2008; Barnes and Hartmann, 2010; Athanasiadis *et al.*, 2010) recent studies have explicitly analysed the nature of the eddy-driven jet to understand the wintertime variability. Woollings *et al.* (2010a) found that the North Atlantic eddy-driven jet exhibits three preferred latitudinal positions during winter, closely related to the variability of the NAO and East Atlantic patterns. The tri-modal distribution of the eddy-driven jet was found to be a robust characteristic of the variability throughout the twentieth century (Woollings *et al.*, 2014). Franzke *et al.* (2011) demonstrated that the most common transitions between the three eddy-driven jet regimes involve consistent Rossby wave-breaking and associated momentum convergence, similar to wave-breaking behaviour in idealised experiments (e.g. Orlanski, 2003; Rivière, 2009) and to that associated with the

different phases of the NAO (Rivière and Orlanski, 2007; Martius *et al.*, 2007).

Recently, the dominant transitions of the North Atlantic eddy-driven jet position have been linked to variability of storm-track activity in the upstream region. Ambaum and Novak (2014) suggest that the storm track activity in the western North Atlantic is akin to a nonlinear oscillator. They showed that periods of intense storm track activity are often followed by periods of lower activity, during which the baroclinicity increases, leading to another period of intense storm track activity, and so on. Novak *et al.* (2015) showed that the storm track cycle upstream is closely linked to the preferred transitions of the eddy-driven jet. Periods of intense storm track activity upstream tend to shift the jet to the northern position, followed by a period of lower storm track activity and increasing baroclinicity when the jet tends to be located first in the southern regime and then the middle jet regime, where the baroclinicity peaks.

During winter, the restoration of the strong baroclinicity in the western North Atlantic can primarily be attributed to upstream orography and land–sea temperature contrast, but the sharp Gulf Stream sea-surface temperature (SST) gradient is also important (Brayshaw *et al.*, 2009, 2011). The strong Gulf Stream SST gradient acts to increase the local baroclinicity through intense sensible and latent heat fluxes, and also anchors an intense precipitation band (e.g. Minobe *et al.*, 2008, 2010; Kuwano-Yoshida *et al.*, 2010b). Evidence for the influence of sharp SST gradients on storm track position and intensity has emerged in studies using idealised models (e.g. Brayshaw *et al.*, 2008; Nakamura *et al.*, 2008; Sampe *et al.*, 2010; Deremble *et al.*, 2012; Ogawa *et al.*, 2012), more realistic models (Woollings *et al.*, 2010b) as well as observations (Qiu *et al.*, 2014; O'Reilly and Czaja, 2015).

In this article we investigate the influence of the Gulf Stream on the North Atlantic eddy-driven jet and its variability. To do this we analyse a pair of atmospheric general circulation model (AGCM) simulations, forced with realistic and smoothed Gulf Stream SST boundary conditions, and compare these results with a reanalysis dataset. A similar approach has been used in the study by Small *et al.* (2014), analysing the mean storm track response, and Piazza *et al.* (2015), who investigated the response in the marine boundary layer as well as the response of the large-scale circulation. The storm track response over the Gulf Stream is found to be somewhat larger amplitude in the study by Small *et al.* (2014), using the Community Atmosphere Model version 4 (CAM-4) model, than in the study of Piazza *et al.* (2015), using the ARPEGE* model, for comparable SST smoothing. Piazza *et al.* (2015) find that the response of the mean jet to the SST small-scale features consists of a weakening of the westerlies over Europe, a strengthening of the North Atlantic eddy-driven jet on the poleward flank, and a slight strengthening of the subtropical jet over Africa.

The simulations analysed here were previously used to investigate the influence of the Gulf Stream on wintertime blocking over Europe (O'Reilly *et al.*, 2016). The Gulf Stream was found to be important in intensifying the storm track during the period prior to the onset of European blocking, the result being a higher frequency of blocking. Now we wish to investigate how the Gulf Stream, through its influence on the storm track, affects the wintertime eddy-driven jet over the North Atlantic region, upstream of the European blocking region. However, the relationship between European blocking and North Atlantic jet variability will also be analysed later in the article.

The AGCM simulations, reanalysis dataset and methods are explained in more detail in section 2. In section 3 we assess the influence of the Gulf Stream on the mean eddy-driven jet and storm track. The presence of the sharp Gulf Stream SST front leads to more intense lower-tropospheric meridional heat transport in the western North Atlantic, as in previous studies, but here it is demonstrated that this is coincident with a more poleward mean eddy-driven jet. To better understand the difference between the two simulations, we analyse the variability of the eddy-driven jet in the two experiments in section 4. In section 5 we analyse the relationship between the storm track intensity and jet position. A summary and further discussion follow in section 6.

2. Methods

2.1. Model simulations and reanalysis data

In this study we analyse the results of two contrasting 20-year AGCM simulations which were performed using the 'AGCM for Earth Simulator (version 3)' (AFES) model, developed and run at the Japan Agency for Marine–Earth Science and Technology (Ohfuchi *et al.*, 2004; Enomoto *et al.*, 2008; Kuwano-Yoshida *et al.*, 2010b). The model set-up is similar to that used by Minobe *et al.* (2008) and Kuwano-Yoshida *et al.* (2010a), who analysed a 5-year integration of the previous version of the AFES model. The version of the AGCM used in this study has previously been used to analyse explosively deepening extratropical cyclones in ensemble forecasts (Kuwano-Yoshida, 2014; Kuwano-Yoshida and Enomoto, 2014) and the development of European blocking (O'Reilly *et al.*, 2016). The model has a horizontal resolution of T239 (∼50 km) and 48 sigma levels in the vertical. The model employs the Emanuel convection scheme (e.g. Emanuel and Zivkovic-Rothman, 1999). We analyse the AFES output on a 0.5° horizontal grid at 6 hourly interval.

For the lower boundary condition, the time-varying NOAA Optimally Interpolated (AVHRR-only) daily SST (Reynolds *et al.* 2007) is used from September 1981 to August 2001. The control simulation was performed using the SST boundary condition as provided in the dataset (hereafter referred to as CONTROL); the second simulation used the SST data smoothed over the Gulf Stream region by applying a 1-2-1 running mean filter in both the zonal and meridional directions 200 times on the 0.25° grid in the region 85 to 30°W, 25–50°N (hereafter referred to as SMOOTH). Climatological DJF SST contours from these simulations are shown in Figure 1.

The AGCM simulations are compared with data from the National Centers for Environmental Predition Climate Forecast System Reanalysis (hereafter NCEP-CFSR) dataset from 1979 to 2009, which is provided on a 0.5° grid at 6 h intervals (Saha *et al.*, 2010).

A 2–8 day band-pass Lanczos filter (Duchon, 1979) is used throughout to calculate the eddy statistics.

2.2. North Atlantic eddy-driven jet latitude

To analyse the variability of the eddy-driven jet position, we follow the method of Woollings *et al.* (2014), which is similar to the method used in Woollings *et al.* (2010a). The daily mean zonal wind at 850 hPa is first zonally averaged between 0 and 60°W over the North Atlantic. A 10-day low-pass Lanczos filter (Duchon, 1979) is then applied before selecting the latitude of the maximum zonal wind at each day in the resulting time series (between 20 and 75°N). Following the method used in Woollings *et al.* (2010a), we estimate the probability density functions (PDFs) using the kernel method of Silverman (1981), with smoothing parameter $h = 1.06\sigma n^{-1/5}$. Here σ is the standard deviation and n is the sample size. The same method is also used to calculate the PDFs of the lower-tropospheric meridional eddy heat transport over the western North Atlantic.

2.3. Significance tests

The statistical significance of the difference plots (CONTROL minus SMOOTH) in section 3 and the PDF difference plots in section 4 is estimated using a Monte Carlo resampling method.

*Action de Recherche Petite Echelle Grande Echelle.

The statistics for each winter in CONTROL and SMOOTH are combined and randomly split into two sets of 20 winters and the difference between the random samples is saved. The process is repeated 10 000 times to assess the probability that the difference between the datasets could occur at random. From these distributions we calculate the 5 and 10% significance levels of a two-sided test, corresponding to the top or bottom 2.5 and 5 percentiles of the distribution, respectively.

The significance of the difference between the composite time series of the jet latitude and **E** vector forcing in section 5 were produced using a similar technique. The individual heat flux events that make up the CONTROL and SMOOTH composites were shuffled and randomly resampled 10 000 times to calculate the 5 and 10% significance levels of a two-sided test.

The significance of the blocking frequency during the upper tercile of eddy heat flux period (shown in Figure 10 below) was calcuated by randomly shuffling the years of the blocking index and recalculating using the same heat-flux timeseries, then repeating 10 000 times to estimate the significance of the blocking frequency anomaly. This method was also used to calculate the significance of the composite geopotential height anomalies during the upper-tercile eddy heat flux events and European blocking development, shown in Figure 12 below.

3. Jet and storm track climatologies

We begin by analysing the influence of the Gulf Stream on the climatological mean North Atlantic eddy-driven jet. The eddy-driven jet can be well visualised by the zonal wind velocity at 850 hPa (e.g. Woollings *et al.*, 2014) which we will use as our measure of the eddy-driven jet. At 850 hPa, the eddy-driven jet is well separated from the subtropical jet, which is strongest in the upper troposphere. The shading in Figure 1 shows the wintertime climatologies of the zonal velocity, at 850 hPa, in the NCEP-CFSR, CONTROL and SMOOTH, as well as the difference between the two simulations (defined here and throughout as CONTROL minus SMOOTH). The zonal velocity at 850 hPa exhibits a peak at the eastern edge of the Gulf Stream and exhibits a slight southwest–northeast tilt. The AGCM simulations approximately capture the qualitative structure of the mean eddy-driven jet, however the magnitude of the flow in both simulations is slightly stronger than in NCEP-CFSR. In CONTROL, the mean eddy-driven jet exhibits a slightly more tilted structure than SMOOTH and also appears to be stronger over the eastern edge of the Gulf Stream and further polewards. The difference map indicates that the eddy-driven jet in CONTROL exhibits a significant, albeit modest, poleward shift compared to the eddy-driven jet in SMOOTH, which is more zonal and exhibits stronger westerlies over western and central Europe.

Also shown in Figure 1 are the zonal wind climatologies at 300 hPa. There is little difference between the two simulations in the upper-level jet over the western Atlantic region, where the jet is subtropical in nature with little signature at the surface. However, futher downstream, where the jet is more barotropic, the differences in the upper-level winds match the differences in the lower-level wind, indicating that the experiments have a significantly different eddy-driven jet, which has a signature in both the upper and lower troposphere. The weaker jet over western Europe in CONTROL is consistent with the findings in O'Reilly *et al.* (2016), in which the same simulations are found to exhibit more frequent blocking anomalies over Europe. The jet response to the Gulf Stream seen in our simulations is to some extent corroborated by the results of Piazza *et al.* (2015) (their Figure 8). Piazza *et al.* also found a poleward shift of the eddy-driven jet with realistic compared to smoothed SSTs, however the differences are largest over the middle of the North Atlantic and there is no significant jet response downstream over continental Europe in their simulations, where the differences in our simulations are most significant (i.e. Figure 1(d)). To investigate how the presence of the Gulf Stream generates the more northern eddy-driven jet position, we will now analyse the storm track activity over the North Atlantic.

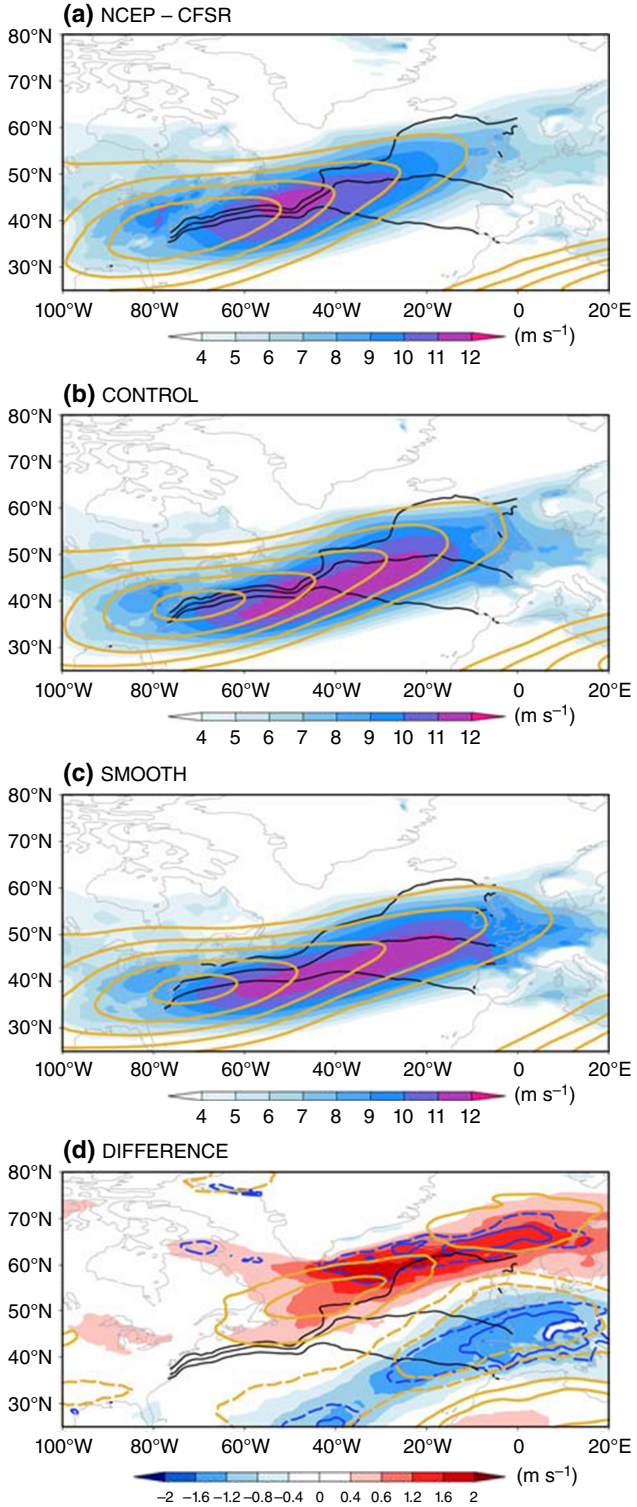

Figure 1. Wintertime (DJF) climatologies of the zonal velocity at 850 hPa (shading) and at 300 hPa (contours) in (a) NCEP-CFSR, (b) CONTROL and (c) SMOOTH. (d) shows the difference (defined as CONTROL minus SMOOTH), where the dashed and solid blue contours indicate where the difference is significant at the 10 and 5% levels respectively. Zonal velocity at 300 hPa is contoured every 5 m s^{-1} from 20 m s^{-1} in (a), (b) and (c). In (d), the zonal velocity difference is contoured at −3, −1.5, 1.5 and 3 m s^{-1}, where the negative contours are dashed. SST contours for each dataset are drawn in black at 8, 12 and 16 °C (the observations are also shown in (d) for reference).

Anticipating that the local influence of the Gulf Stream will be primarily in the lower troposphere, we will first analyse the meridional heat transport by baroclinic eddies, which is an effective measure of growing baroclinic waves (e.g. Simmons and Hoskins, 1978) and was explicitly linked to the downstream

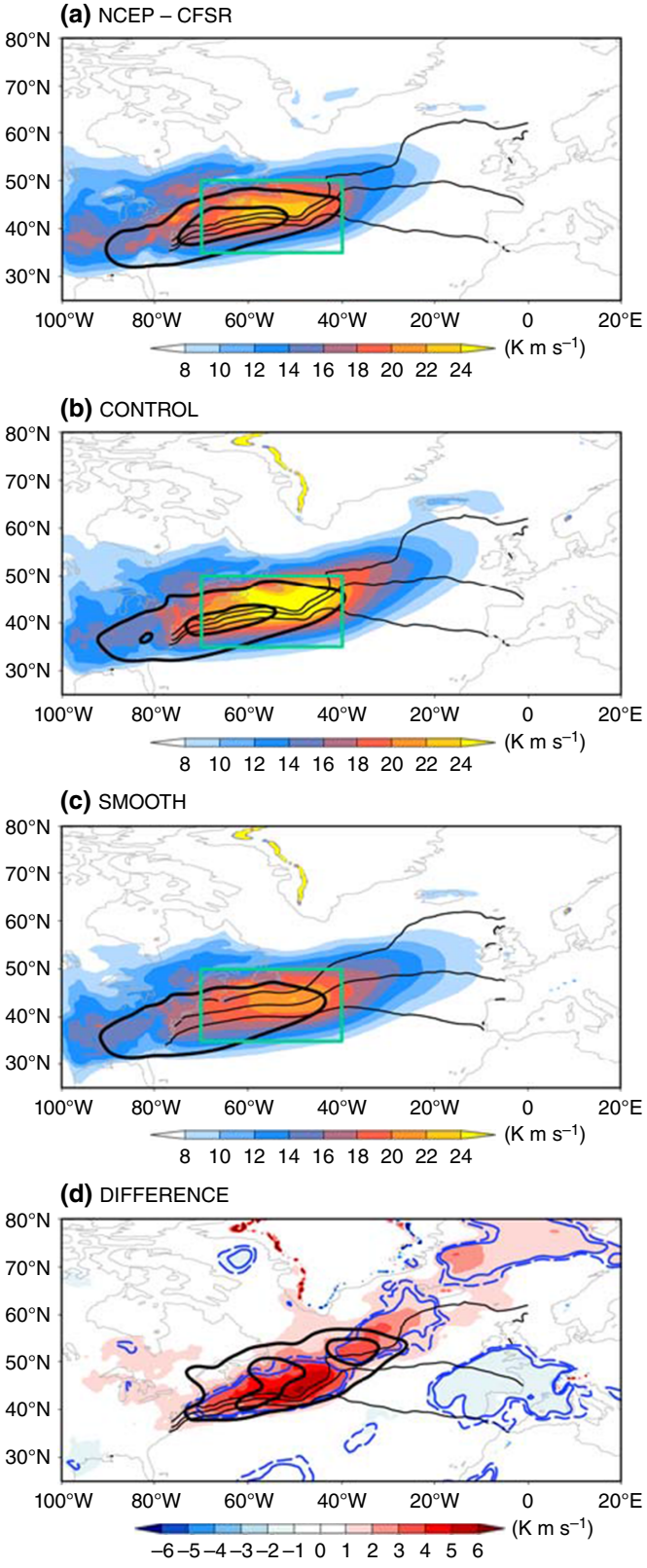

Figure 2. Wintertime (DJF) climatologies of the meridional eddy heat flux, $\overline{v'T'}$, at 850 hPa (shading) in (a) NCEP-CFSR, (b) CONTROL and (c) SMOOTH. (d) shows the difference (defined as CONTROL minus SMOOTH), where the dashed and solid blue contours indicate where the difference is significant at the 10 and 5% levels respectively. The Eady growth rate at 775 hPa is shown in bold black contours at 0.65 and 0.75 day^{-1} for NCEP-CFSR, at 0.35 and 0.45 day^{-1} for CONTROL and SMOOTH and at 0.02 and 0.04 day^{-1} for the DIFFERENCE plot. The SSTs for each dataset are drawn in thin black contours at 8, 12 and 16 °C (the observations are shown in (d) for reference).

eddy-driven jet variability by Novak *et al.* (2015). Figure 2 shows the wintertime climatologies of the meridional eddy heat transport, $\overline{v'T'}$, at 850 hPa. In the NCEP-CFSR, meridional eddy heat transport peaks along the north side of the Gulf Stream SST front, reflecting the anchoring effect of the Gulf Stream SST front observed in other studies (e.g. Brayshaw *et al.*, 2011; Small *et al.*, 2014). Similarly, the meridional eddy heat transport in CONTROL exhibits a peak along the north side of the Gulf Stream SST front but is stronger than in the NCEP-CFSR. The meridional eddy heat transport in SMOOTH is significantly weaker than in CONTROL, particularly over the Gulf Stream region where the heat transport is about 25% larger, as emphasised in the difference map (Figure 2(d)), consistent with Small *et al.* (2014). The difference map also shows a weak dipole pattern in the meridional eddy heat transport further downstream, likely reflecting the shift in eddy-driven jet position. It is important to emphasise that the largest difference in the meridional eddy heat transport between the two simulations is found considerably further upstream of the largest difference in the eddy-driven jet (i.e. Figure 1(d)), suggesting downstream influence of the increased storm track activity over the Gulf Stream.

The climatological Eady growth rate, $\sigma_E = 0.31(f/N)\partial U/\partial Z$, is also shown in bold black contours in Figure 2. We calculated the Eady growth rate at the 775 hPa level, following Hoskins and Valdes (1990). This provides a measure of the lower-level baroclinicity of the large-scale flow, which is found to peak upstream of the midlatitude storm tracks (e.g. Hoskins and Valdes, 1990; Ambaum and Novak, 2014). The AGCM simulations both largely underestimate σ_E compared to reananlysis data but is about 10% larger over the Gulf Stream region in the CONTROL simulation than in SMOOTH. This is qualitatively consistent with the larger meridional eddy heat transport found in the CONTROL simulation than in the SMOOTH simulation.

4. Variability of eddy-driven jet and storm track

Analysis of the climatologies suggests the presence of the sharp Gulf Stream SST front results in both a northward shift in the mean eddy-driven jet and intensified local meridional eddy heat transport. However, it remains unclear if increased storm track activity in the lower troposphere can be linked to a poleward shift in the eddy-driven jet by analysing the climatologies alone. A study by Novak *et al.* (2015) has shown that, during periods when the meridional eddy heat transport over the Gulf Stream is strong, the eddy-driven jet tends to be in a more northern position. This would suggest that the presence of the Gulf Stream SST front could generate a more northern mean eddy-driven jet through increased meridional eddy heat transport. To try to understand how the Gulf Stream SST front acts to generate a more poleward eddy-driven jet, we now analyse the variability of the eddy-driven jet latitude and the lower-tropospheric storm track activity over the Gulf Stream region.

To measure the variability of the eddy-driven jet position, we identify the latitude of the peak low-pass filtered zonal velocity averaged over the North Atlantic, broadly following methods used in previous studies of the North Atlantic eddy-driven jet (e.g. Woollings *et al.*, 2010a, 2014; Franzke and Woollings, 2011; Franzke *et al.*, 2011; Hannachi *et al.*, 2012). This method is described in section 2. Figure 3(a) shows the PDFs of the eddy-driven jet latitude in the NCEP-CFSR, CONTROL and SMOOTH. The NCEP-CSFR exhibits the tri-modal distribution as found in previous studies of the North Atlantic eddy-driven jet (e.g. Woollings *et al.*, 2010a), however the period of NCEP-CFSR (i.e. 1979–2009) exhibits a more pronounced skew towards the northern position than earlier periods in the 20th century (Woollings *et al.*, 2014). The CONTROL simulation similarly exhibits a tri-modal distribution, however the position of the southern jet peak is slightly further north and occurs more

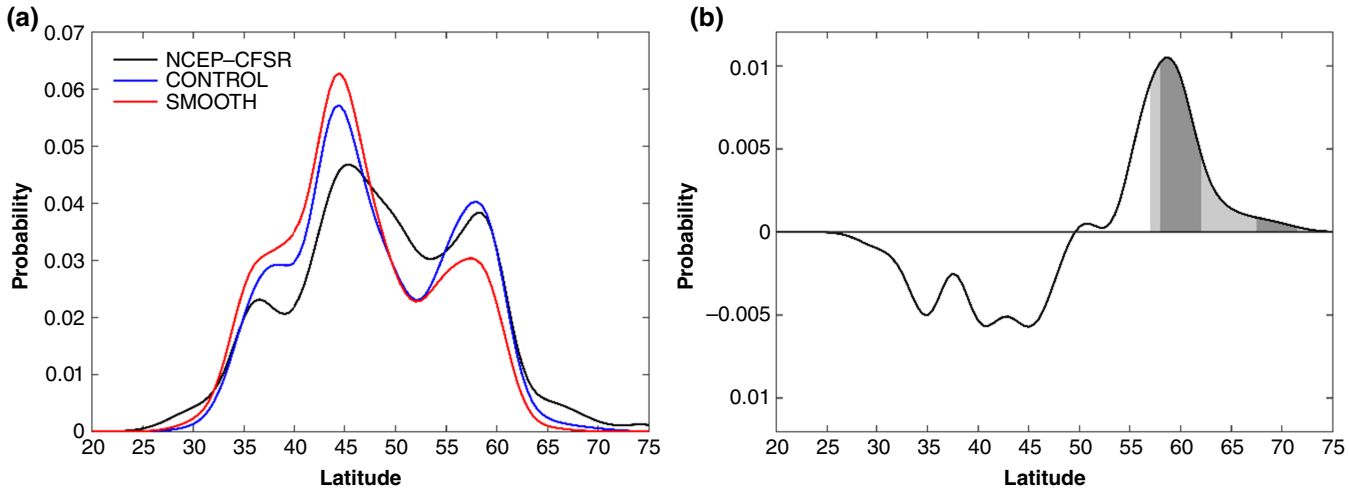

Figure 3. (a) Climatological PDFs of the wintertime eddy-driven jet latitude in NCEP-CFSR, CONTROL and SMOOTH. (b) Difference between the PDFs in (a) for the two experiments (i.e. CONTROL minus SMOOTH), where the light and dark grey shading indicates where the difference is significant at the 10 and 5% levels respectively.

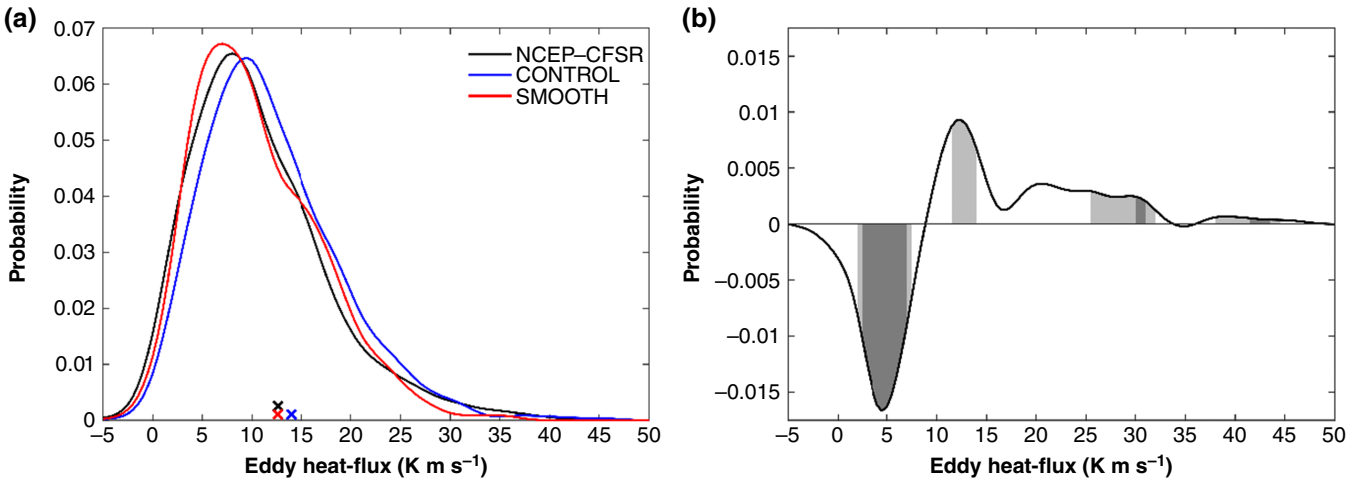

Figure 4. (a) Climatological PDFs of the 10 day low-pass-filtered index of meridional eddy heat flux (i.e. $v'T'_{850\text{hPa}}$), averaged over the Gulf Stream region (shown in Figure 2), in NCEP-CFSR, CONTROL and SMOOTH. (b) Difference between the PDFs in (a) for the two experiments (i.e. CONTROL minus SMOOTH), where the light and dark grey shading indicates where the difference is significant at the 10 and 5% levels respectively. The crosses in (a) indicate the value of the upper tercile threshold in each dataset.

frequently than in the NCEP-CFSR[†]. The central jet position in CONTROL also occurs more frequently than in the NCEP-CFSR, however the frequency of the northern jet position is very well captured. A notable feature of CONTROL is that the northern and central jet peaks are more distinct than in NCEP-CFSR. The jet in SMOOTH occurs more frequently at the southern and central jet locations than in NCEP-CFSR and CONTROL. As such, the tri-modal jet distribution seen in the NCEP-CFSR and CONTROL is weakened in SMOOTH. However, the northern eddy-driven jet position in SMOOTH does closely correspond to the northern jet location in both NCEP-CFSR and CONTROL, albeit about 25% less frequently. The difference between the jet latitude distributions in CONTROL and SMOOTH is shown in Figure 3(b). As already highlighted, the northern jet occurs significantly more frequently in CONTROL than in SMOOTH, indicating that the more poleward location of the climatological eddy-driven jet in the CONTROL experiment (i.e. Figure 1) is due to a more frequent northern jet position rather than, for example, a northward shift of the entire distribution of eddy-driven jet latitude.

To understand the role of the storm track activity in the variability of the eddy-driven jet latitude, we first consider the variability of the storm track activity. Based on maps of the mean meridional eddy heat transport, shown in Figure 2, it seems plausible that the increase in frequency of northern jet occurrence may be as a result of the increased upstream storm track activity, consistent with the findings of Novak *et al.* (2015). To test this, we follow the method of Novak *et al.* (2015) and use a 10-day low-pass filtered index (using a Lanczos filter, as before) of the meridional eddy heat transport at 850 hPa between 35 and 50°N, 70 and 40°W, as shown on the climatological maps in Figure 2.

Figure 4(a) shows the distributions of the meridional eddy heat transport over the Gulf Stream region in NCEP-CFSR, CONTROL and SMOOTH and Figure 4(b) shows the difference between the AGCM experiments. Comparing the three distributions in Figure 4(a), it is immediately apparent that the peak in the distribution of SMOOTH is found at lower values than in CONTROL and NCEP-CFSR. Analysing the difference between CONTROL and SMOOTH distributions, it is clear that the CONTROL simulation has a significantly longer tail, reflecting occurrences of very high meridional eddy heat transport in the CONTROL simulation. This is important because the skewed distribution indicates that the Gulf Stream SST gradient is not only responsible for a stronger mean storm track intensity but also for periods of extremely high heat flux that are essentially non-existent in its absence.

[†]Not many models have been able to capture the trimodal distribution, for example none of the CMIP5 control simulations demonstrate the trimodal structure adequately (Anstey *et al.*, 2013), however some more recent models have been shown to improve the distribution (Williams *et al.*, 2015).

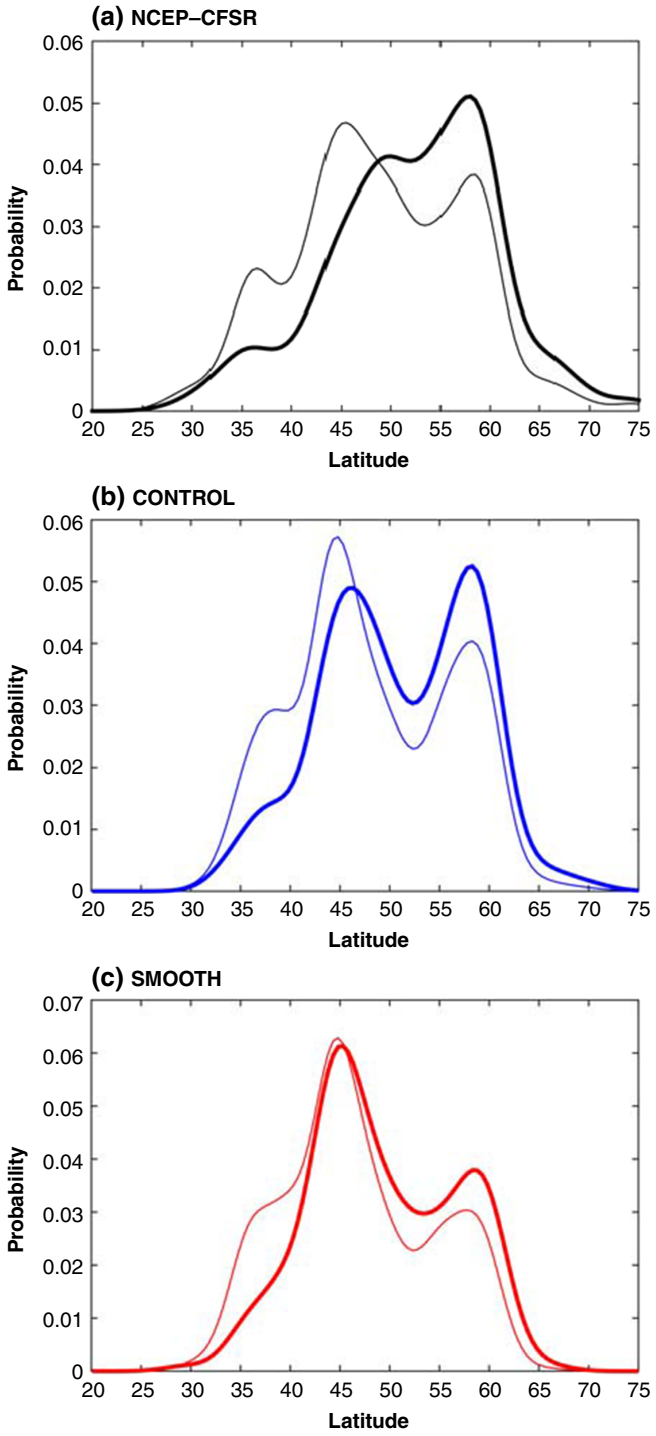

Figure 5. PDFs of the eddy-driven jet latitude during periods of high eddy heat flux (i.e. $v'T'_{850\text{hPa}}$) over the Gulf Stream region, defined as being in the upper-tercile of the distributions in Figure 4, for (a) NCEP-CFSR, (b) CONTROL and (c) SMOOTH. Bold lines indicate the high heat flux periods and the thin lines are the climatological PDFs, as shown in Figure 3(a).

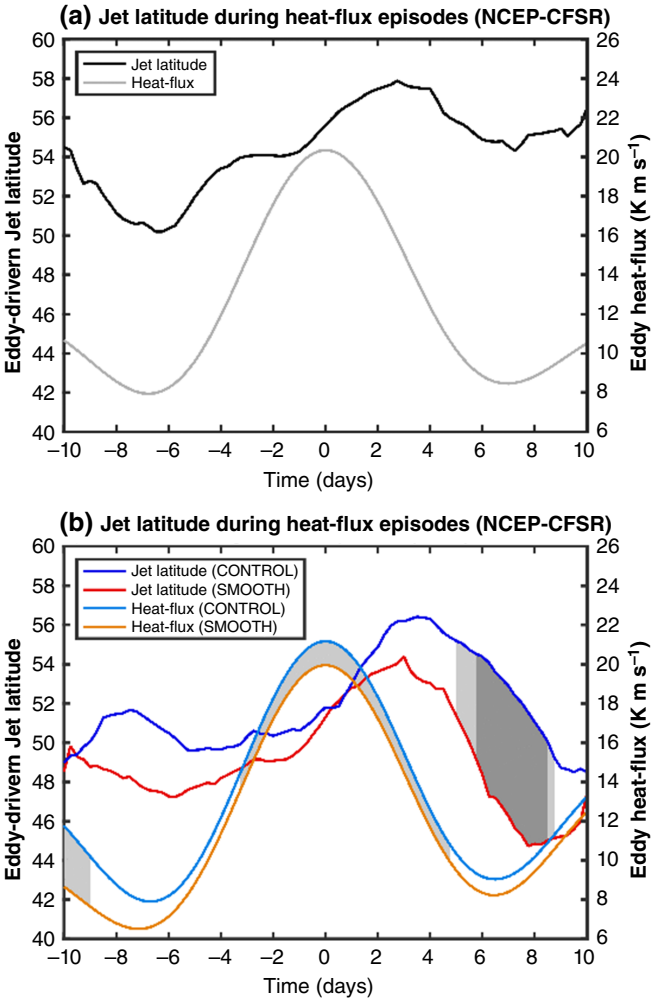

Figure 6. Composites of the eddy-driven jet latitude evolution during high heat flux (i.e. $v'T'_{850\text{hPa}}$) events over the Gulf Stream region in (a) NCEP-CFSR and (b) CONTROL and SMOOTH. The time series are centred on the time of the peaks in the (10-day low-pass-filtered) index of the eddy heat flux over the Gulf Stream region. The time series of composite jet latitude have been smoothed using a 3-day moving average. The light and dark grey shading in (b) indicates where the composites are significantly different at the 10 and 5% levels respectively. Whilst the difference between the heat flux at each time step around the peak time (i.e. $t = 0$) is only significant at the 10% level, the difference between the heat flux averaged between −3 and +3 days is significant at the 5% level.

5. Influence of storm track intensity on jet position

To investigate the link between the meridional eddy heat transport over the Gulf Stream region and eddy-driven jet latitude, we now analyse the eddy-driven jet behaviour during periods of high meridional eddy heat transport, defined here as the upper tercile of each distribution shown in Figure 4(a). The upper tercile thresholds are 12.62, 13.92 and 12.58 K m s^{-1} in the NCEP-CFSR, CONTROL and SMOOTH respectively. The distributions of the eddy-driven jet latitude during high heat-flux periods are shown in Figure 5. The eddy-driven jet occupies the northern position more regularly than any other latitude during high heat flux periods in NCEP-CFSR, occurring about 30% more often than in the climatology. Similarly, the northern position is also occupied about 30% more frequently in the CONTROL simulation. The jet in the SMOOTH simulation occurs most frequently in the central position in the high heat flux period, though the frequency of the northern position is slightly increased. Despite this, it is clear that, even in the SMOOTH simulation, periods of high meridional eddy heat flux over the Gulf Stream region are concurrent with more frequent northern jet migrations in the downstream region.

Using the index of eddy heat flux over the Gulf Stream region, we can narrow our focus to analyse the behaviour of the eddy-driven jet following high heat flux events in the upstream region. To do this, we produce composites of the jet latitude, centred on peaks in the eddy heat flux indices that occur in the upper tercile, excluding peaks that occur within 10 days of a larger one, with the resulting composites consisting of 125 events in NCEP-CFSR, 90 events in CONTROL and 80 events in SMOOTH. Figure 6 shows composites of the jet latitude during the evolution of these high heat flux events. In the NCEP-CFSR, the latitude of the jet migrates northwards as the upstream eddy heat flux increases and exhibits a substantial polewards shift following the peak in the eddy heat flux. The composite jet remains within the northern region for around a week. In the AFES simulations, the eddy heat flux is, as expected, higher in the CONTROL events than SMOOTH ones. Following the peak in eddy heat flux over the

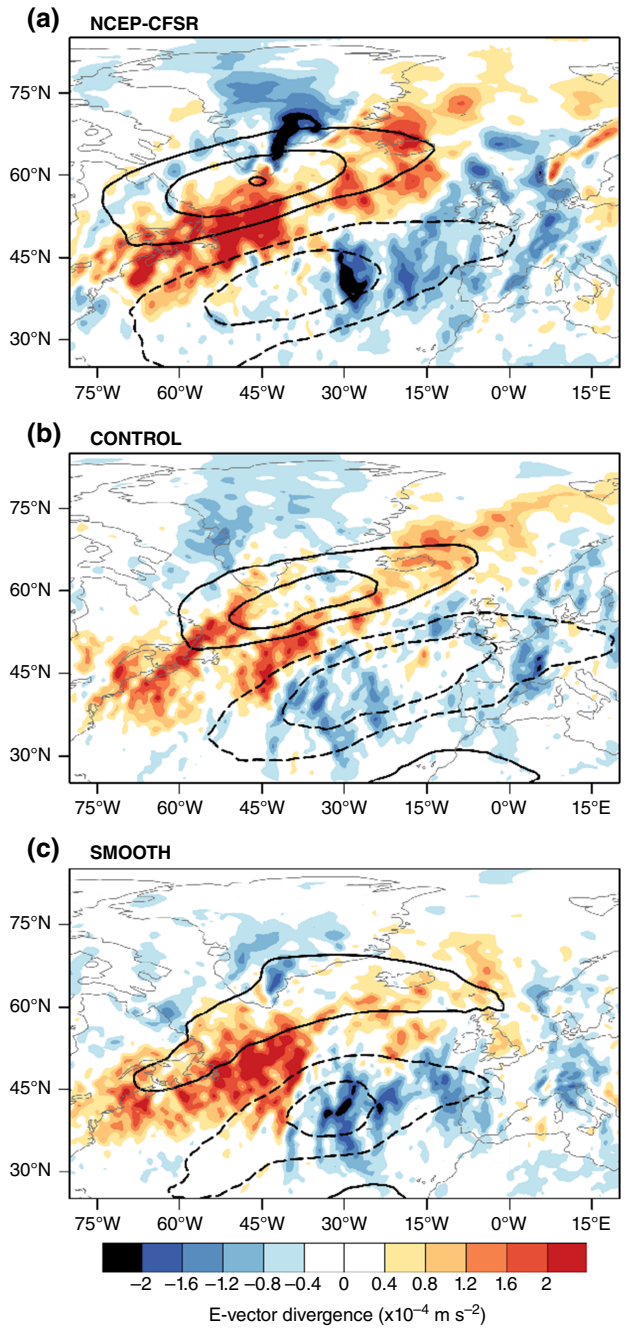

Figure 7. Composite divergence of the horizontal **E** vector at 300 hPa (shading) for the high heat flux events, averaged from −1 to +2 days relative to the peak in eddy heat flux (i.e. Figure 6), for (a) NCEP-CFSR, (b) CONTROL and (c) SMOOTH. The zonal velocity anomaly averaged over the same period is contoured at −9, −6, −3, 3, 6 and 9 m s^{-1}, where negative values are indicated by dashed contours. The zonal velocity anomalies in the CONTROL and SMOOTH are taken relative to a combined climatology.

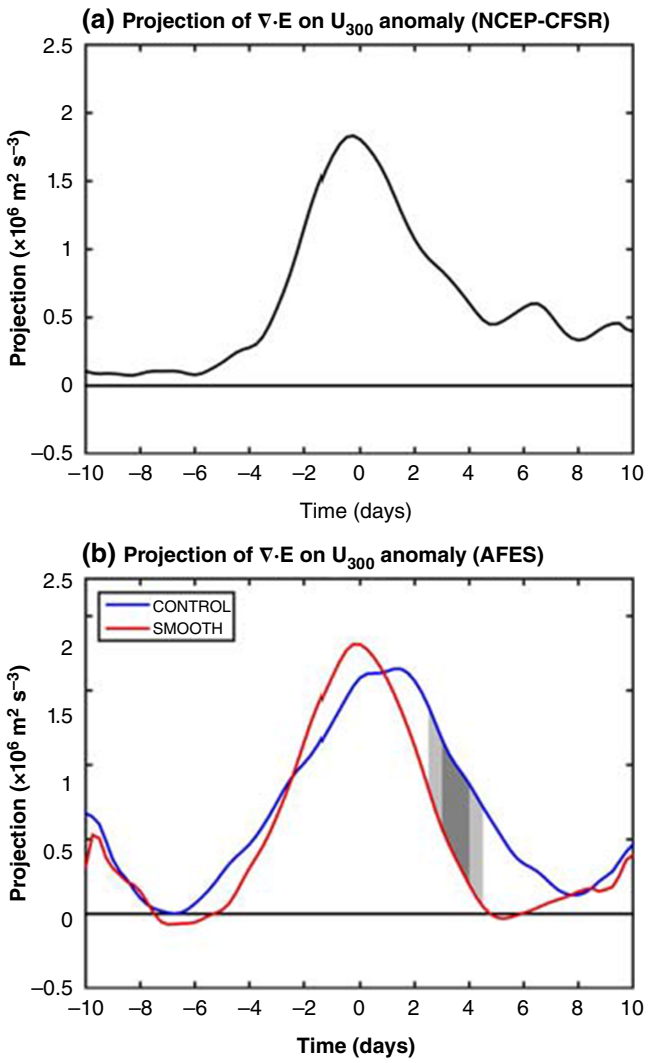

Figure 8. Time series of the composite 300 hPa horizontal **E** vector divergence onto the normalised zonal wind anomaly associated with the northward jet shift (i.e. the zonal wind anomaly averaged between −1 and +2 days shown in Figure 7), in (a) NCEP-CFSR and (b) CONTROL and SMOOTH. The light and dark grey shading in (b) indicates where the composites are significantly different at the 10 and 5% levels respectively. The time series have been smoothed using a 3-day moving average prior to the computation of the composites and significance.

Gulf Stream region, as in NCEP-CFSR, the eddy-driven jet shifts polewards in both CONTROL and SMOOTH, however the jet moves further polewards in the CONTROL simulation. However, the most significant difference between the two experiments is that the jet remains in a northern position for significantly longer in the CONTROL simulation, on the order of a week or so, whereas in the SMOOTH simulation the jet shifts north for only a few days following the heat flux peak.

The higher number of northern jet periods in CONTROL than in SMOOTH are associated with high heat flux periods over the Gulf Stream region, which are significantly larger and more frequent. However, it is not clear why the eddy-driven jet remains significantly further north, and for longer, in the period following high heat flux events in the CONTROL simulation. Woollings *et al.* (2011) analysed the evolution of poleward jet shifts and showed that they were accompanied by eddy momentum fluxes in the upper troposphere acting over the northern part of the Euro-Atlantic sector to move the jet polewards as well as maintain it there for a week or more. To analyse the role of eddy momentum fluxes, we follow Woollings *et al.* (2011) and produce composites of the **E** vector (Hoskins *et al.*, 1983) during the high eddy heat flux events in each of the datasets. The divergence of the **E** vector provides a measure of the velocity tendency due to eddy momentum fluxes in the time-mean (or low-pass) zonal momentum equation (Hoskins *et al.*, 1983). Maps of the composite **E** vector divergence averaged between −1 and +2 days relative to the peak of the high heat flux events are shown in Figure 7. The zonal velocity anomalies at 300 hPa are also plotted for reference. Here, the zonal velocity anomalies in CONTROL and SMOOTH are calculated relative to a combined mean in order to provide an unbiased result. The **E** vector divergence is somewhat similar in all datasets, projecting onto the positive zonal velocity anomaly over the North Atlantic, however the zonal velocity anomalies are weaker in SMOOTH. The large values of the **E** vector divergence extend past Iceland in both NCEP-CFSR and CONTROL, whereas in SMOOTH the anomalies are predominantly confined to the western Atlantic region.

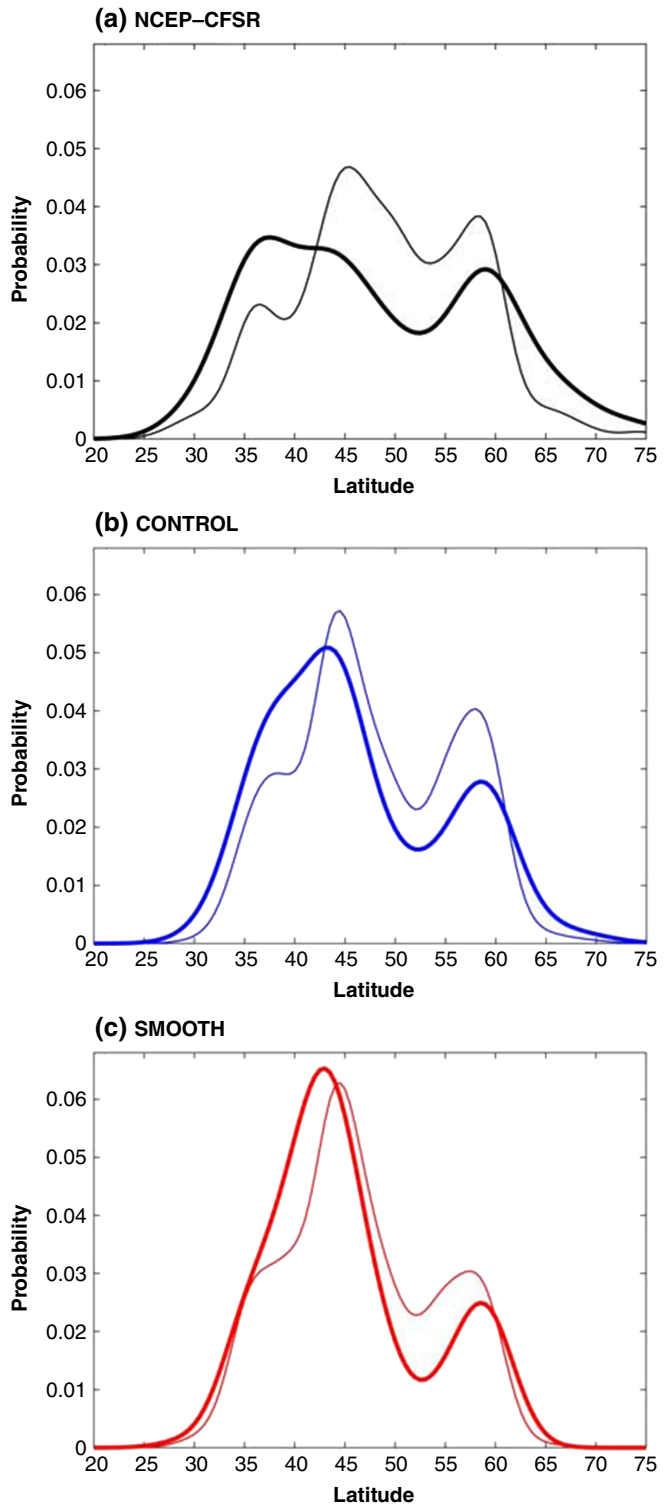

Figure 9. PDFs of the eddy-driven jet latitude during periods of European blocking (between 20°W and 40°E, using indices calculated in O'Reilly *et al.* (2016) for (a) NCEP-CFSR, (b) CONTROL and (c) SMOOTH. Bold lines indicate the European blocking periods and the thin lines are the climatological PDFs, as shown in Figure 3(a).

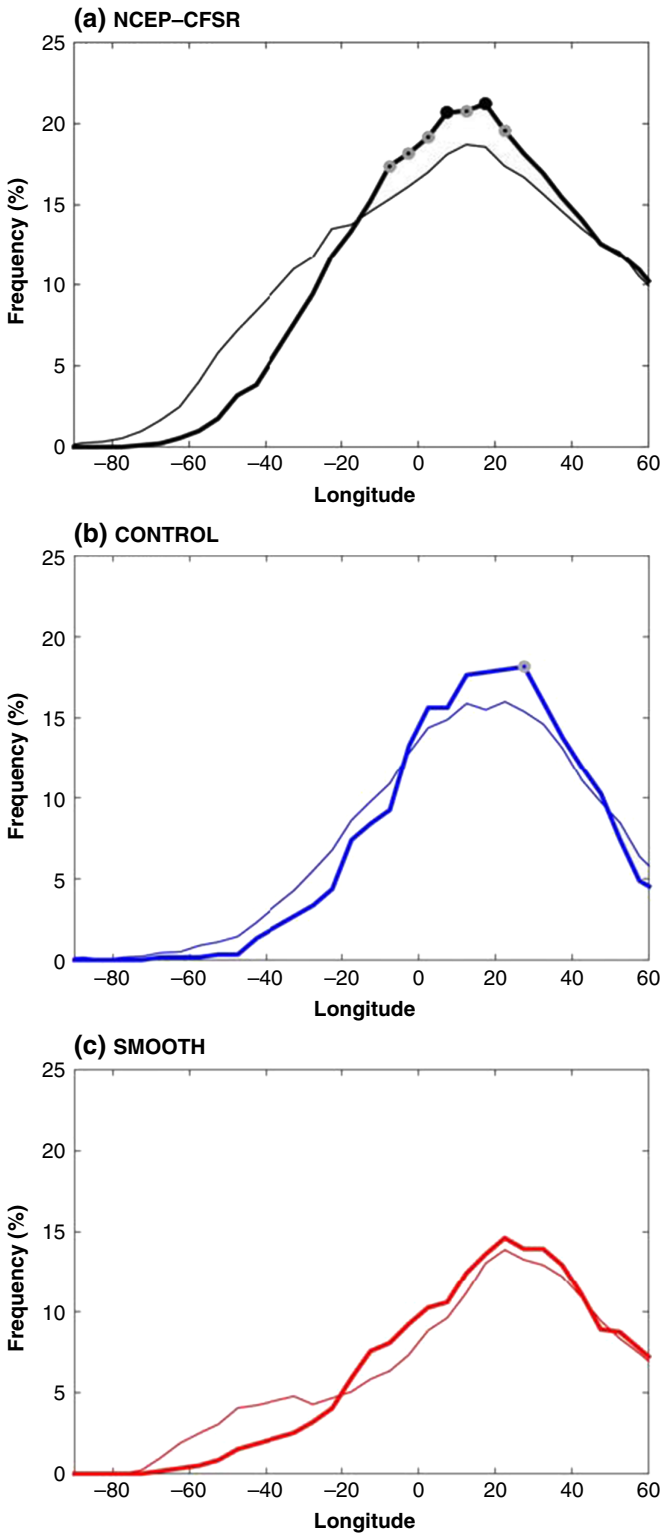

Figure 10. Wintertime midlatitude blocking frequency, using the blocking indices calculated in O'Reilly *et al.* (2016), during the upper tercile of heat flux over the Gulf Stream region (thick lines) and climatologies (thin lines): (a) NCEP-CFSR, (b) CONTROL and (c) SMOOTH. The grey and black circles indicate regions where the blocking frequency anomaly during the upper tercile is significant at the 10 and 5% levels respectively.

To visualise the evolution of the **E** vector forcing during high heat flux events, we projected the **E** vector divergence onto the zonal velocity anomaly fields shown in Figure 7 over the North Atlantic sector (75°W–15°E, 20°N–90°N). Prior to computing the projection, the composite zonal velocity anomaly fields (i.e. the contours in Figure 7) were normalised by dividing the area-averaged velocity anomaly amplitude, such that the time series represent the impact of the eddies alone. The time series of the **E** vector evolution are shown in Figure 8. In NCEP-CFSR, the magnitude of the **E** vector forcing on the northern jet shift peaks at same time as the eddy heat flux over the Gulf Stream. The **E** vector forcing remains anomalously large for over a week, acting to maintain the jet in the northern jet position (i.e. Figure 6(a)), similar to the composite jet shift in Woollings *et al.* (2011). In the AGCM experiments, the **E** vector forcing peaks at about the same time as the eddy heat flux but interestingly the **E** vector forcing in the CONTROL experiment remains anomalously large for about a week, significantly longer than in the SMOOTH simulation. In fact, the lesser impact of the high-heat flux events

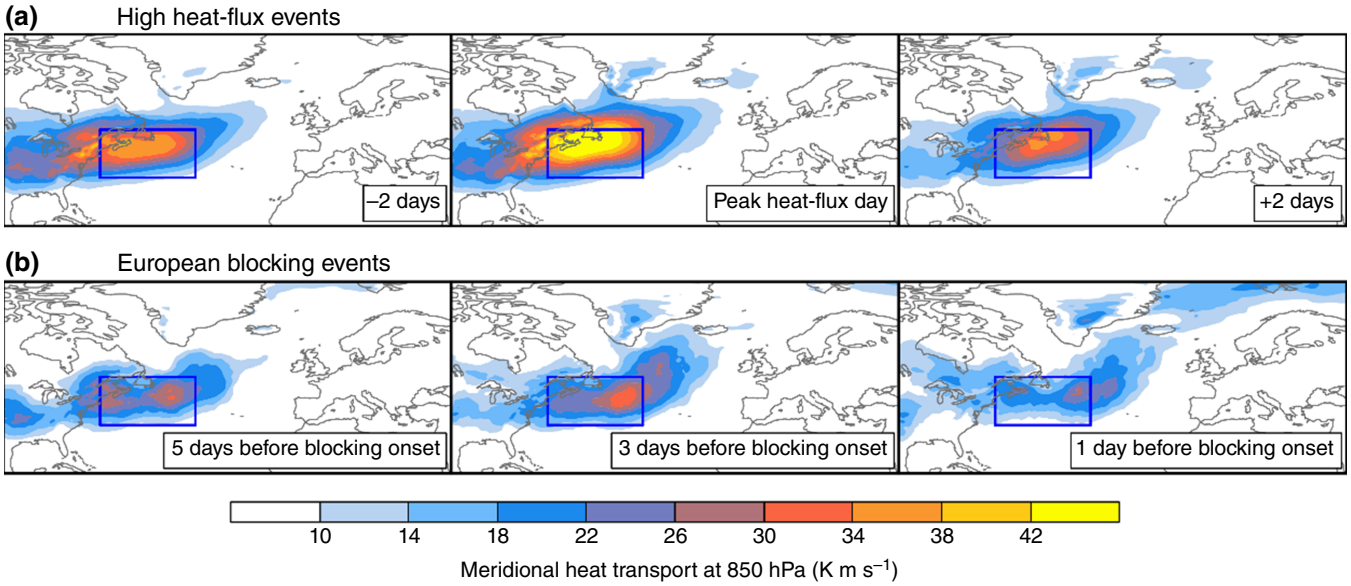

Figure 11. Evolution of the 3-day averaged meridional eddy heat transport (i.e. $v'T'$) at 850 hPa during (a) the 125 highest heat flux events and (b) the development of the 31 European blocking events analysed by O'Reilly *et al.* (2016). The labels indicate the central time of the 3 day average. The meridional eddy heat flux during the development of European blocking is largest at approximately 3 days before blocking onset. The box in each panel indicates the region over which the meridional eddy heat transport index is computed over the western North Atlantic.

on the downstream jet in SMOOTH can even be seen in Figure 7, where the **E** vector divergence is confined to the western Atlantic region. This is consistent with the jet remaining in the northern position for significantly longer in the CONTROL simulation, showing that the eddies more actively maintain the jet in the northern position in the CONTROL simulation where there are higher eddy heat fluxes in the Gulf Stream region. Based on these plots, the eddy heat flux over the Gulf Stream region (which depends crucially on the strong SST gradient) is not only important for the initial poleward shift of the jet, but also for generating sufficiently strong upper-tropospheric eddy activity. This activity in turn acts to maintain the jet in the northern position further downstream and reinforce the zonal velocity anomalies.

6. Summary and discussion

In this article we have investigated the influence of the Gulf Stream SST front on the North Atlantic eddy-driven jet and its variability. The AGCM simulations analysed were forced with realistic (CONTROL) and smoothed (SMOOTH) Gulf Stream SST boundary conditions. With the smoothed SST gradient, the meridional eddy heat flux in the lower troposphere is weaker and the eddy-driven jet is further downstream over the eastern North Atlantic, compared to the the AGCM simulation with the realistically strong SST front. The CONTROL simulation is found to more accurately capture the trimodal distribution of the eddy-driven jet latitude, than in the SMOOTH simulation, with the more poleward climatological jet being the result of the jet occupying the northern jet position more frequently.

Previously, Novak *et al.* (2015) showed that the northern jet location of the North Atlantic jet tends to be associated with periods of high meridional eddy heat flux over the Gulf Stream region. The larger frequency of the northern jet location in the CONTROL simulation is similarly associated with periods of high eddy heat flux over the Gulf Stream region, however the increase in northern jet position in the SMOOTH simulation is comparitively small, consistent with the weaker eddy heat flux over the Gulf Stream region. Composites of high heat flux events reveal that the significantly higher heat flux is followed by larger and more persistient poleward jet excursions in CONTROL than in SMOOTH. Analysis of the upper-tropospheric eddy momentum fluxes demonstrates that, in CONTROL, a stronger eddy feedback acts to maintain the more poleward eddy-driven jet.

Recently, it was found that, in the same AGCM simulations, blocking frequency over Europe is significantly improved in CONTROL (O'Reilly *et al.*, 2016). Davini *et al.* (2014) suggested that the northern jet position tends to be associated with blocking over Europe, so it is possible that the poleward jet displacement results are directly linked to the greater frequency of European blocking in CONTROL. To test whether this is the case, we calculated the distribution of the eddy-driven jet latitude during periods of midlatitude European blocking (as calculated in O'Reilly *et al.*, 2016), which is plotted in Figure 9. During European blocking there appears to be an actual reduction in the frequency of the northern jet position with another peak further south, which likely represents a split jet over the North Atlantic. This distribution is similar to that seen in Woollings *et al.* (2010a), despite the results presented here not being directly comparable due to the different algorithms, datasets, region and period used. The jet distribution during European blocking events shows that the more frequent total occurrence of the northern jet location in CONTROL does not simply reflect the higher frequency of European blocking. However, that is not to say that these are unrelated.

It was demonstrated in O'Reilly *et al.* (2016) that strong eddy heat fluxes along the Gulf Stream tend to occur prior to large-scale upper tropospheric wave-breaking and the onset of European blocking. Therefore more frequent higher eddy heat flux events over the Gulf Stream region could be consistent with both increased European blocking frequency and poleward eddy-driven jet displacement. To analyse this, the midlatitude blocking frequency (again, as calculated in O'Reilly *et al.*, 2016) is shown in Figure 10 for the upper tercile of eddy heat flux periods over the Gulf Stream region and the wintertime climatology. During the upper tercile of eddy heat flux over the Gulf Stream region, blocking frequency over Europe exhibits similar increases in NCEP-CFSR and CONTROL (although the increase in the CONTROL is not significant, likely due to the relatively short 20-year simulation). In particular, the NCEP-CFSR shows a significant increase in blocking frequency over Europe, indicating that the storm track intensity upstream is linked to both poleward jet displacements over the North Atlantic and large-scale midlatitude blocking events further downstream over Europe.

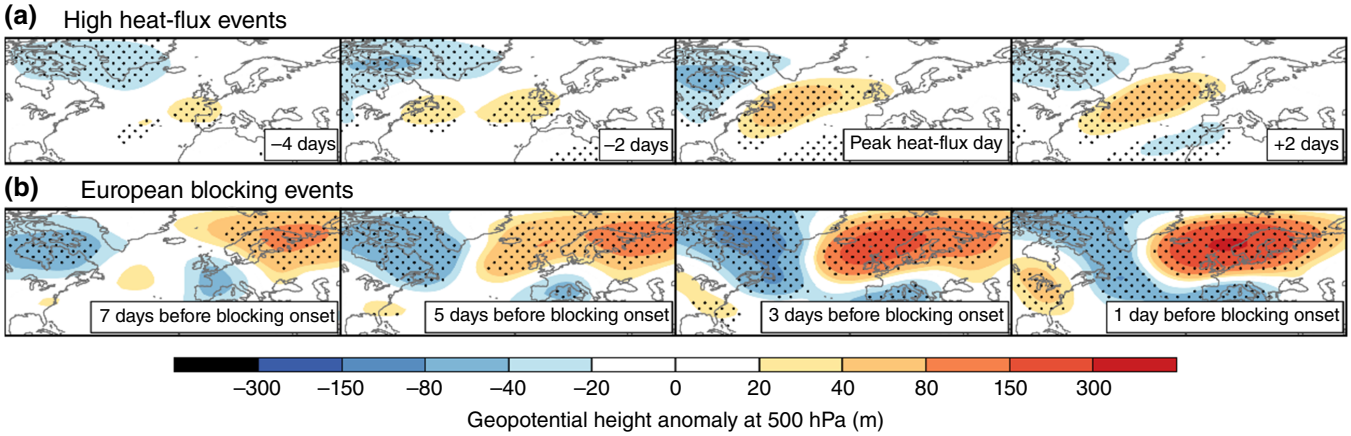

Figure 12. Evolution of the 3-day averaged 500 hPa geopotential height anomalies during (a) the 125 high heat flux events and (b) the development of the 31 European blocking events analysed by O'Reilly *et al.* (2016). The labels indicate the central time of the 3-day average. The stippling indicates regions where the composite anomalies are significant at the 5% level.

The importance of high heat flux events over the Gulf Stream region during the development of both European blocking and poleward jet displacements leads us to question what is different between these two types of event. It could be that the high heat flux events differ in nature and governs how the large-scale flow evolves, or that there is a pre-existence of a large-scale Rossby wave anomaly downstream (e.g. Michel and Rivière, 2011). To address this question, we have produced composite maps of the evolution of meridional eddy heat transport, shown in Figure 11, during the development of the 125 high heat flux events (analysed in section 5) and the 31 European blocking events analysed in O'Reilly *et al.* (2016), using the NCEP-CFSR dataset. The clearest difference between the two types of event is that the high heat flux events have a stronger peak heat flux because these events were selected based on heat flux over the Gulf Stream region. The peak eddy heat flux during the development of European blocking events occurs further downstream than the peak during the high heat flux events. This potentially explains why the ridge that develops into the blocking anomaly over Europe occurs further downstream than the poleward jet displacement, which occurs further west over the North Atlantic Ocean.

Composite maps of the 500 hPa geopotential height anomalies during the development of the high heat flux events and European blocking events are shown in Figure 12. Seven days before the onset of European blocking, there is already a significant positive geopotential height anomaly over eastern Europe, which appears to be a precursor that promotes the development of European blocking, reminiscent of the Rossby wave precursor highlighted by Michel and Rivière (2011) and Nakamura *et al.* (1997). During the development of the high heat flux events (and subsequent poleward jet displacement) there is no significantly positive geopotential height anomaly over eastern Europe. However, there is a weak but apparently significant negative geopotential height anomaly over Greenland. This is consistent with the jet being closer to the central position prior to the poleward jet shift that follows the high heat flux event, which is consistent with the preferential jet transition from the central to northern jet postition which has been highlighted in previous studies (e.g. Franzke *et al.*, 2011). This suggests that both the pre-existing ridge over eastern Europe and the high heat flux over the eastern side of the Gulf Stream region are important for the development of European blocking. The heat flux over the eastern side of the Gulf Stream region is much reduced in the SMOOTH simulation and results in significantly less blocking over Europe and the blocking anomalies that do occur develop in a different manner to that observed in reanalysis data (O'Reilly *et al.*, 2016).

It has previously been shown that models which poorly capture the frequency of blocking over Europe tend to be associated with biases which are too zonal in the mean jet stream (Scaife *et al.*, 2010) and storm track (Zappa *et al.*, 2014). Scaife *et al.* (2011) highlighted that the blocking over Europe is significantly improved when the SST biases are reduced over the Gulf Stream region, but these biases largely reflect the incorrect position of the Gulf Stream axis, particularly over the region where the Gulf Stream SST front becomes more meridionally aligned, around 45°W. As such, the 'too zonal' nature of the Atlantic jet in many of the CMIP5 models may, to some extent, be related to the poor capture of the forcing of the overlying storm track by the strong SST gradients in the Gulf Stream region.

Acknowledgements

The authors are grateful to Gwendal Rivière for his insightful comments and suggestions. This work was supported by the Japan Society for the Promotion of Science (Grant-in-Aid for Scientific Research 22106008, 26287110) and the UK Natural Environment Research Council (grant number NE/M005887/1).

References

Ambaum MH, Novak L. 2014. A nonlinear oscillator describing storm track variability. *Q. J. R. Meteorol. Soc.* **140**: 2680–2684.

Anstey JA, Davini P, Gray LJ, Woollings TJ, Butchart N, Cagnazzo C, Christiansen B, Hardiman SC, Osprey SM, Yang S. 2013. Multi-model analysis of Northern Hemisphere winter blocking: Model biases and the role of resolution. *J. Geophys. Res.: Atmos.* **118**: 3956–3971, doi: 10.1002/jgrd.50231.

Athanasiadis PJ, Wallace JM, Wettstein JJ. 2010. Patterns of wintertime jet stream variability and their relation to the storm tracks. *J. Atmos. Sci.* **67**: 1361–1381.

Barnes EA, Hartmann DL, 2010. Dynamical feedbacks and the persistence of the NAO. *J. Atmos. Sci.* **67**: 851–865.

Brayshaw DJ, Hoskins B, Blackburn M. 2008. The storm-track response to idealized SST perturbations in an aquaplanet GCM. *J. Atmos. Sci.* **65**: 2842–2860.

Brayshaw DJ, Hoskins BJ, Blackburn M. 2009. The basic ingredients of the North Atlantic storm track. Part I: Land–sea contrast and orography. *J. Atmos. Sci.* **66**: 2539–2558.

Brayshaw DJ, Hoskins B, Blackburn M. 2011. The basic ingredients of the North Atlantic storm track. Part II: Sea surface temperatures. *J. Atmos. Sci.* **68**: 1784–1805.

Davini P, Cagnazzo C, Fogli PG, Manzini E, Gualdi S, Navarra A. 2014. European blocking and Atlantic jet stream variability in the NCEP/NCAR reanalysis and the CMCC-CMS climate model. *Clim. Dyn.* **43**: 71–85.

Deremble B, Lapeyre G, Ghil M. 2012. Atmospheric dynamics triggered by an oceanic SST front in a moist quasi-geostrophic model. *J. Atmos. Sci.* **69**: 1617–1632.

Duchon CE. 1979. Lanczos filtering in one and two dimensions. *J. Appl. Meteorol.* **18**: 1016–1022.

Eichelberger SJ, Hartmann DL. 2007. Zonal jet structure and the leading mode of variability. *J. Clim.* **20**: 5149–5163.

Emanuel KA, Živkovic-Rothman M. 1999. Development and evaluation of a convection scheme for use in climate models. *J. Atmos. Sci.* **56**: 1766–1782.

Enomoto T, Kuwano-Yoshida A, Komori N, Ohfuchi W. 2008. Description of AFES 2: Improvements for high-resolution and coupled simulations. In *High-Resolution Numerical Modelling of the Atmosphere and Ocean*, Hamilton K, Ohfuchi W (eds.): 77–97. Springer: Berlin.

Franzke C, Woollings T. 2011. On the persistence and predictability properties of North Atlantic climate variability. *J. Clim.* **24**: 466–472.

Franzke C, Woollings T, Martius O. 2011. Persistent circulation regimes and preferred regime transitions in the North Atlantic. *J. Atmos. Sci.* **68**: 2809–2825.

Hannachi A, Woollings T, Fraedrich K. 2012. The North Atlantic jet stream: A look at preferred positions, paths and transitions. *Q. J. R. Meteorol. Soc.* **138**: 862–877.

Held IM, Hou AY. 1980. Nonlinear axially symmetric circulations in a nearly inviscid atmosphere. *J. Atmos. Sci.* **37**: 515–533.

Hoskins BJ, James IN, White GH. 1983. The shape, propagation and mean-flow interaction of large-scale weather systems. *J. Atmos. Sci.* **40**: 1595–1612.

Hoskins BJ, Valdes PJ. 1990. On the existence of storm-tracks. *J. Atmos. Sci.* **47**: 1854–1864.

Kuwano-Yoshida A. 2014. Using the local deepening rate to indicate extratropical cyclone activity. *SOLA* **10**: 199–203.

Kuwano-Yoshida A, Enomoto T. 2014. Predictability of explosive cyclogenesis over the northwestern Pacific region using ensemble reanalysis. *Mon. Weather Rev.* **141**: 3769–3785.

Kuwano-Yoshida A, Enomoto T, Ohfuchi W. 2010a. An improved PDF cloud scheme for climate simulations. *Q. J. R. Meteorol. Soc.* **136**: 1583–1597.

Kuwano-Yoshida A, Minobe S, Xie S-P. 2010b. Precipitation response to the Gulf Stream in an atmospheric GCM. *J. Clim.* **23**: 3676–3698.

Li C, Wettstein JJ. 2012. Thermally driven and eddy-driven jet variability in reanalysis. *J. Clim.* **25**: 1587–1596.

Lorenz DJ, Hartmann DL. 2003. Eddy-zonal flow feedback in the Northern Hemisphere winter. *J. Clim.* **16**: 1212–1227.

Martius O, Schwierz C, Davies H. 2007. Breaking waves at the tropopause in the wintertime Northern Hemisphere: Climatological analyses of the orientation and the theoretical LC1/2 classification. *J. Atmos. Sci.* **64**: 2576–2592.

Michel C, Rivière G. 2011. The link between Rossby wave breakings and weather regime transitions. *J. Atmos. Sci.* **68**: 1730–1748.

Minobe S, Kuwano-Yoshida A, Komori N, Xie S-P, Small RJ. 2008. Influence of the Gulf Stream on the troposphere. *Nature* **452**: 206–209.

Minobe S, Miyashita M, Kuwano-Yoshida A, Tokinaga H, Xie S-P. 2010. Atmospheric response to the Gulf Stream: Seasonal variations. *J. Clim.* **23**: 3699–3719.

Nakamura H, Nakamura M, Anderson JL. 1997. The role of high-and low-frequency dynamics in blocking formation. *Monthly Weather Review* **125**: 2074–2093.

Nakamura H, Sampe T, Goto A, Ohfuchi W, Xie S-P. 2008. On the importance of midlatitude oceanic frontal zones for the mean state and dominant variability in the tropospheric circulation. *Geophys. Res. Lett.* **35**: L15709, doi: 10.1029/2008GL034010.

Novak L, Ambaum MH, Tailleux R. 2015. The life cycle of the North Atlantic storm track. *J. Atmos. Sci.* **72**: 821–833.

Ogawa F, Nakamura H, Nishii K, Miyasaka T, Kuwano-Yoshida A. 2012. Dependence of the climatological axial latitudes of the tropospheric westerlies and storm tracks on the latitude of an extratropical oceanic front. *Geophys. Res. Lett.* **39**: L05804, doi: 10.1029/2011GL049922.

Ohfuchi W, Nakamura H, Yoshioka MK, Enomoto T, Takaya K, Peng X, Yamane S, Nishimura T, Kurihara Y, Ninomiya K. 2004. 10 km mesh meso-scale resolving simulations of the global atmosphere on the Earth Simulator: Preliminary outcomes of AFES (AGCM for the Earth Simulator). *J. Earth Simulator* **1**: 8–34.

O'Reilly CH, Czaja A. 2015. The response of the Pacific storm track and atmospheric circulation to Kuroshio Extension variability. *Q. J. R. Meteorol. Soc.* **141**: 52–66.

O'Reilly CH, Minobe S, Kuwano-Yoshida A. 2016. The influence of the Gulf Stream on wintertime European blocking. *Clim. Dyn.* **47**: 1545–1567, doidoi: 10.1007/s00382-015-2919-0.

Orlanski I. 2003. Bifurcation in eddy life cycles: Implications for storm track variability. *J. Atmos. Sci.* **60**: 993–1023.

Piazza M, Terray L, Boé J, Maisonnave E, Sanchez-Gomez E. 2015. Influence of small-scale North Atlantic sea surface temperature patterns on the marine boundary layer and free troposphere: A study using the atmospheric Arpege model. *Clim. Dyn.* **46**: 1699–1717. doi: 10.1007/s00382-015-2669-z.

Qiu B, Chen S, Schneider N, Taguchi B. 2014. A coupled decadal prediction of the dynamic state of the Kuroshio Extension system. *J. Clim.* **27**: 1751–1764.

Reynolds RW, Smith TM, Liu C, Chelton DB, Casey KS, Schlax MG. 2007. Daily high-resolution-blended analyses for sea surface temperature. *J. Clim.* **20**: 5473–5496.

Rivière G. 2009. Effect of latitudinal variations in low-level baroclinicity on eddy life cycles and upper-tropospheric wave-breaking processes. *J. Atmos. Sci.* **66**: 1569–1592.

Rivière G, Orlanski I. 2007. Characteristics of the Atlantic storm-track eddy activity and its relation with the North Atlantic Oscillation. *J. Atmos. Sci.* **64**: 241–266.

Saha S, Moorthi S, Pan H-L, Wu X, Wang J, Nadiga S, Tripp P, Kistler R, Woollen J, Behringer D, Liu H, Stokes D, Grumbine R, Gayno G, Wang J, Hou Y-T, Chuang H-Y, Juang H-MH, Sela J, Iredell M, Treadon R, Kleist D, Van Delst P, Keyser D, Derber J, Ek M, Meng J, Wei H, Yang R, Lord S, Van Den Dool H, Kumar A, Wang W, Long C, Chelliah M, Xue Y, Huang B, Schemm J-K, Ebisuzaki W, Lin R, Xie P, Chen M, Zhou S, Higgins W, Zou C-Z, Liu Q, Chen Y, Han Y, Cucurull L, Reynolds RW, Rutledge G, Goldberg M. 2010. The NCEP climate forecast system reanalysis. *Bull. Am. Meteorol. Soc.* **91**: 1015–1057.

Sampe T, Nakamura H, Goto A, Ohfuchi W. 2010. Significance of a midlatitude SST frontal zone in the formation of a storm track and an eddy-driven westerly jet. *J. Clim.* **23**: 1793–1814.

Scaife AA, Woollings T, Knight J, Martin G, Hinton T. 2010. Atmospheric blocking and mean biases in climate models. *J. Clim.* **23**: 6143–6152.

Scaife AA, Copsey D, Gordon C, Harris C, Hinton T, Keeley S, O'Neill A, Roberts M, Williams K. 2011. Improved Atlantic winter blocking in a climate model. *Geophys. Res. Lett.* **38**: L23703, doi: 10.1029/2011GL049573.

Silverman BW. 1981. Using kernel density estimates to investigate multimodality. *J. R. Stat. Soc. Ser. B* **43**: 97–99.

Simmons AJ, Hoskins BJ. 1978. The life cycles of some nonlinear baroclinic waves. *J. Atmos. Sci.* **35**: 414–432.

Small RJ, Tomas RA, Bryan FO. 2014. Storm track response to ocean fronts in a global high-resolution climate model. *Clim. Dyn.* **43**: 805–828.

Vallis GK, Gerber EP. 2008. Local and hemispheric dynamics of the North Atlantic Oscillation, annular patterns and the zonal index. *Dyn. Atmos. Oceans* **44**: 184–212.

Williams KD, Harris CM, Bodas-Salcedo A, Camp J, Comer RE, Copsey D, Fereday D, Graham T, Hill R, Hinton T, Hyder P, Ineson S, Masato G, Milton SF, Roberts MJ, Rowell DP, Sanchez C, Shelly A, Sinha B, Walters DN, West A, Woollings T, Xavier PK. 2015. The Met Office Global Coupled model 2.0 (GC2) configuration. *Geosci. Model Dev.* **8**: 1509–1524.

Woollings T, Hannachi A, Hoskins BJ. 2010a. Variability of the North Atlantic eddy-driven jet stream. *Q. J. R. Meteorol. Soc.* **136**: 856–868.

Woollings T, Hoskins BJ, Blackburn M, Hassell D, Hodges K. 2010b. Storm track sensitivity to sea surface temperature resolution in a regional atmosphere model. *Clim. Dyn.* **35**: 341–353.

Woollings T, Pinto JG, Santos JA. 2011. Dynamical evolution of North Atlantic ridges and poleward jet stream displacements. *J. Atmos. Sci.* **68**: 954–963.

Woollings T, Czuchnicki C, Franzke C. 2014. Twentieth century North Atlantic jet variability. *Q. J. R. Meteorol. Soc.* **140**: 783–791.

Zappa G, Masato G, Shaffrey L, Woollings T, Hodges K. 2014. Linking Northern Hemisphere blocking and storm track biases in the CMIP5 climate models. *Geophys. Res. Lett.* **41**: 135–139, doi: 10.1002/2013GL058480.